



UNIVERSITY OF LEEDS

This is a repository copy of *Observation of a New Channel, the Production of CH₃, in the Abstraction Reaction of OH Radicals with Acetaldehyde*.

White Rose Research Online URL for this paper:
<http://eprints.whiterose.ac.uk/104218/>

Version: Accepted Version

Article:

Howes, NUM, Lockhart, JPA, Blitz, MA orcid.org/0000-0001-6710-4021 et al. (6 more authors) (2016) Observation of a New Channel, the Production of CH₃, in the Abstraction Reaction of OH Radicals with Acetaldehyde. *Physical Chemistry Chemical Physics*, 18 (38). pp. 26423-26433. ISSN 1463-9076

<https://doi.org/10.1039/C6CP03970G>

© the Owner Societies 2016. This is an author produced version of a paper published in *Physical Chemistry Chemical Physics*. Uploaded in accordance with the publisher's self-archiving policy.

Reuse

Items deposited in White Rose Research Online are protected by copyright, with all rights reserved unless indicated otherwise. They may be downloaded and/or printed for private study, or other acts as permitted by national copyright laws. The publisher or other rights holders may allow further reproduction and re-use of the full text version. This is indicated by the licence information on the White Rose Research Online record for the item.

Takedown

If you consider content in White Rose Research Online to be in breach of UK law, please notify us by emailing eprints@whiterose.ac.uk including the URL of the record and the reason for the withdrawal request.



eprints@whiterose.ac.uk
<https://eprints.whiterose.ac.uk/>

1 **Observation of a New Channel, the Production of CH₃, in the** 2 **Abstraction Reaction of OH Radicals with Acetaldehyde**

3 Neil U. M. Howes, James P. A. Lockhart[†], Mark A. Blitz^{1*}, Scott A. Carr, Maria Teresa Baeza-
4 Romero[‡], Dwayne E. Heard¹, Robin J. Shannon[‡], Paul W. Seakins^{1*} and T. Varga[#]

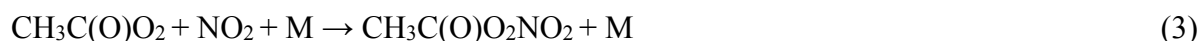
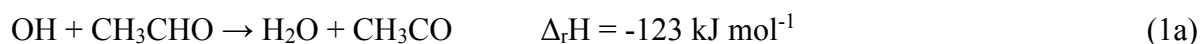
5 School of Chemistry, University of Leeds, Leeds, LS2 9JT, UK.

6 ¹ National Centre for Atmospheric Science, University of Leeds, Leeds, LS2 9JT, UK.

7
8 **ABSTRACT:** Using laser flash photolysis coupled to photo-ionization time-of-flight mass spectrometry
9 (PIMS), methyl radicals (CH₃) have been detected as primary products from the reaction of OH radicals
10 with acetaldehyde (ethanal, CH₃CHO) with a yield of ~15% at 1-2 Torr of helium bath gas. Supporting
11 measurements based on laser induced fluorescence studies of OH recycling in the OH/CH₃CHO/O₂
12 system are consistent with the PIMS study. Master equation calculations suggest that the origin of the
13 methyl radicals is from prompt dissociation of chemically activated acetyl products and hence is
14 consistent with previous studies which have shown that abstraction, rather than addition/elimination, is
15 the sole route for the OH + acetaldehyde reaction. However, the observation of a significant methyl
16 product yield suggests that energy partitioning in the reaction is different from the typical early barrier
17 mechanism where reaction exothermicity is channeled preferentially into the newly formed bond. The
18 master equation calculations predict atmospheric yields of methyl radicals of ~ 14 %. The implications of
19 the observations in atmospheric and combustion chemistry are briefly discussed.

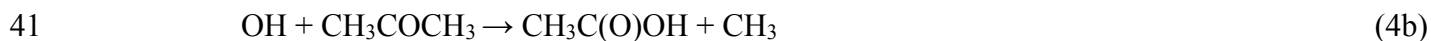
21 **INTRODUCTION**

22 Acetaldehyde (ethanal, CH₃CHO) is an important atmospheric pollutant formed in the oxidation of many
23 hydrocarbons¹ and also a primary pollutant, particularly from ethanol combustion²⁻⁴ and higher alcohols.⁵
24 ⁶ Acetaldehyde has been measured in a number of environments at concentrations of sub ppb in remote
25 regions,⁷ to tens of ppb in polluted cities.⁸⁻¹¹ Acetaldehyde is a potential carcinogen¹² and, via reaction
26 with the OH radical, a significant source of peroxyacetyl nitrate (PAN):



30 PAN is an important component of photochemical smog, a known irritant and a vehicle, via reaction 3,
31 for the long range transport of NO_x in the atmosphere.

32 The kinetics of reaction 1 have been extensively studied; a room temperature rate coefficient of
33 $(1.5 \pm 0.2) \times 10^{-11} \text{ cm}^3 \text{ molecule}^{-1} \text{ s}^{-1}$ has been recommended by IUPAC¹³ and $(1.5 \pm 0.1) \times 10^{-11} \text{ cm}^3$
34 $\text{molecule}^{-1} \text{ s}^{-1}$ in the recent JPL evaluation.¹⁴ Following the observation of an upward curvature of the OH
35 + acetone reaction with decreasing temperature below ~200 K, Wollenhaupt et al.¹⁵ suggested that OH +
36 carbonyl reactions may not be simple abstraction reactions. Based on some product studies, *ab initio*
37 calculations and the established negative temperature dependence of reaction 1, it was suggested that
38 addition/elimination may compete with abstraction for the reactions of OH with carbonyl species.^{16,17} For
39 the reaction of OH with acetone the channels proposed were:



42 For the reaction of OH with acetaldehyde the corresponding channels from addition/elimination would
43 be:



46 However, following the suggestion of an alternative reaction mechanism, a number of product
47 studies were undertaken which appeared to confirm that abstraction was either the dominant, or only,
48 channel in the reaction of OH with carbonyl species, and that the upward curvature with decreasing
49 temperature was not associated with a new reaction channel. For example, Vandenberg and Peeters
50 measured the yield of water following the reaction of OH with acetaldehyde and acetone, reporting a yield
51 of 0.89 ± 0.06 for reaction 1¹⁸ and 0.95 for reaction 4.¹⁹ Butkovskaya et al.²⁰ reported abstraction at ~95%
52 for reaction 1, but determined from observations of the CH₂CHO radical that at 298 K, approximately 5%
53 of the reaction can occur via abstraction from the methyl group of acetaldehyde:



55 Other groups looked for the expected products of addition/elimination and found little evidence to support
56 a substantive alternative to abstraction. Cameron et al.²¹ used UV transient absorption spectroscopy to
57 study both the formation of acetyl (channel 1a) and CH₃ (channel 1b). The primary acetyl yield was
58 determined as 0.93 ± 0.18 . A significant methyl yield was observed, but on a longer timescale than acetyl
59 production, and realistic alternative radical-radical mechanisms for CH₃ production were proposed.
60 However, the acetyl UV spectrum is broad and overlaps with the CH₃ spectrum; therefore, there is

61 potential for incorrect assignment of absorptions, especially if vibrational excitation is present in the
62 radical species. Cameron et al. were also unable to observe any H atom production (using resonance
63 fluorescence techniques). Upper limits of 3% and 2% were put on channels 1b and 1c.

64 Wang et al.²² used IR transient absorption to determine a water yield of ~100% and set an upper
65 limit on CH₃ of 5%, although on the timescale of their reactions, prompt production of CH₃ can occur
66 from the reaction of O(¹D) with acetaldehyde and from some other unknown source. When O₃ was used
67 as the O(¹D) source, a large additional source of CH₃ was observed and attributed to the reaction of acetyl
68 with O₃:



70 In addition, Wang et al. used an indirect method to probe for atomic hydrogen production (1c) and, in
71 agreement with Cameron et al., observed no production setting an upper limit of 5% on channel 1c.

72 There now appears to be a strong consensus that abstraction is the sole mechanism for OH +
73 carbonyl reactions, with recent studies by Shannon et al.^{23, 24} accounting for the increase in the rate
74 coefficient at low temperatures. For reaction 1, acetyl production dominates, but with a small yield of
75 vinoxy radical following abstraction at the methyl group. Finally, the role of water in mediating the
76 reaction has been explored by Vöhringer-Martinez et al.²⁵

77 However, D'Anna et al.²⁶ raised the possibility of a further reaction channel (1e) following
78 abstraction; the production of CH₃ + CO + H₂O, still consistent with 100% H₂O formation, but where
79 some of the acetyl would fragment:



81 Using a smog chamber system, with OH being generated from alkyl nitrite photolysis in synthetic air,
82 D'Anna et al. observed 10% production of CO and HCHO, with HCHO being the expected stable product
83 of methyl radical oxidation in the presence of NO_x. The activation energy of acetyl decomposition is ~71
84 kJ mol⁻¹²⁷ so there is sufficient exothermicity in reaction 1a (-123 kJ mol⁻¹) for acetyl decomposition to
85 occur in a chemically activated process, although this would require deposition of a significant fraction
86 of the reaction exothermicity into the acetyl fragment. Generally abstraction reactions are associated with
87 partitioning exothermicity predominantly into the newly formed bond (H₂O in this case)²⁸, however,
88 D'Anna et al. also carried out *ab initio* calculations which showed that there is a post-reaction complex
89 which might serve to facilitate a more statistical distribution of the reaction exothermicity between the
90 final products. More recent calculations by Mendes et al.²⁹ confirm the presence of a significant post-
91 reaction complex.

92 Experimental support for partitioning reaction exothermicity into spectator bonds comes from our
93 earlier studies on the reaction of OH with methylglyoxal²⁷ and glyoxal.³⁰ Following abstraction of the
94 aldehydic hydrogen atom from methylglyoxal, the resulting CH₃C(O)CO radical is expected to rapidly
95 thermally decompose to acetyl + CO. In the presence of excess oxygen one would then expect to see OH
96 regeneration at low total pressures from the acetyl + O₂ reaction.^{31, 32}



98 OH regeneration was observed, but the Stern Volmer analysis yielded an intercept higher than the expected
99 unity value, suggesting less than 100% acetyl formation. Baeza-Romero et al.²⁷ showed that the observed
100 results could be explained if the CH₃C(O)CO fragment retained sufficient energy not only for initial
101 fragmentation, but additionally for some of the acetyl to decompose, preventing complete OH recycling.
102 Similar conclusions can be drawn from our work on the reaction of OH with glyoxal where prompt
103 decomposition of a fraction of the HC(O)CO prevents OH recycling from the HC(O)CO + O₂ reaction.^{30,}

104 ³³



108 In this current work we have investigated the title reaction with two experimental methodologies.
109 Laser flash photolysis coupled to photoionization mass spectrometry (PIMS)^{34, 35} has been used to
110 positively identify CH₃CO and CH₃ as primary reaction products. At our photoionization energy, CH₃CO
111 fragmentation occurs and CH₃ was detected from acetyl photo-fragmentation, as well as a primary
112 reaction product. Evidence is presented to show that it is possible to differentiate between primary and
113 fragmentation production. To help confirm our findings, we have also used the acetyl + O₂ reaction³² in
114 a similar fashion to our earlier work on methylglyoxal, to show that there is less than 100% acetyl
115 production. This method does not identify the products and only determines the total non-acetyl yield.
116 Finally, we have used the master equation package MESMER³⁶ (Master Equation Solver for Multi-Energy
117 Well Reactions) to explore chemically activated acetyl fragmentation.

118

120 **Laser flash photolysis/photoionization mass Spectrometry Studies**

121 Details of the laser flash photolysis/photoionization mass spectrometry system can be found in the
 122 electronic supplementary information (ESI) and previous publications.^{34,35} Briefly, the system comprised
 123 of a 70 cm long, 1.25 cm diameter, stainless steel flowtube which was illuminated by a pulsed excimer
 124 laser. The OH or Cl radical precursors, substrate and helium bath gas were metered through calibrated
 125 flow controllers and mixed prior to entering the flowtube. The total pressure in the flowtube was
 126 controlled by a rotary pump and measured using a 10 Torr Baratron-type pressure gauge. Experiments
 127 were run with both coated (halocarbon wax) and uncoated flow tubes.

128 The central region of the flowtube passed through an evacuated chamber ($<10^{-5}$ Torr typical
 129 background pressure). A 1 mm hole in the wall of the flowtube allowed the reaction mixture to enter the
 130 chamber where it was exposed to pulsed VUV radiation at 118 nm, generated from frequency tripling 355
 131 nm YAG output, which allowed photoionization of compounds with a threshold ionization energy of less
 132 than 10.5 eV. Ions generated by the VUV laser pulse were focused into a reflectron time of flight mass
 133 spectrometer (ToFMS, Kore Instruments) and were detected via dynode detectors. Ion signals were
 134 monitored on a digital oscilloscope and then passed to a PC for analysis.

135 The time delay between the excimer photolysis laser and the photoionization probe laser was
 136 varied to build up a temporal profile of monitored species with typically two hundred points per trace.
 137 The experiment was allowed to average over 10-15 scans, to increase the signal to noise ratio.

138 Studies were carried out under pseudo-first-order conditions with acetaldehyde in a large excess
 139 over the radical. Under these conditions the acetyl and methyl radicals generated in the flowtube
 140 demonstrated biexponential behavior with a growth determined by the pseudo-first-order rate coefficient
 141 for reaction with acetaldehyde, k'_g , and a loss determined by a combination of removal processes,
 142 primarily diffusion to the flowtube wall which could be approximated to a first-order loss, k_l . The temporal
 143 profile of the ion signal ($S_{X,t}$) is given by equation E1, where the first part of the equation is the bimolecular
 144 profile modified by the sampling process and the second part of the equation allows for any prompt
 145 production of acetyl or methyl.

$$146 \quad S_{X, t} = \frac{S k_g k_{\text{eff}}}{k_l - k_g} \left[\frac{e^{-k_g t} - e^{-k_{\text{eff}} t}}{k_{\text{eff}} - k_g} - \frac{e^{-k_l t} - e^{-k_{\text{eff}} t}}{k_{\text{eff}} - k_l} \right] + \frac{S_{\text{instant}} k_{\text{eff}}}{k_{\text{eff}} - k_l} \left[\frac{e^{-k_l t} - e^{-k_{\text{eff}} t}}{k_{\text{eff}} - k_l} \right] + S_0 \quad (\text{E1})$$

147 S is proportional to the maximum height of the signal, k_g is the coefficient rate of growth of the signal, k_l
 148 is the rate coefficient for the loss rate, k_{eff} is the rate of effusion into the mass spectrometer, S_{instant} refers

149 to any instantaneous observed (photolytic), S_0 is the signal at time zero, and t is time. Typical CH_3 and
150 CH_3CO signal traces from reaction 1 (where $S_{\text{instant}}=0$) are shown in Figure 1.

151

152 **Branching ratios from kinetic studies with excess oxygen**

153 This component of the work has been carried out in two conventional slow-flow, laser flash photolysis,
154 laser induced fluorescence (LIF) apparatus that have been used in several previous publications.^{2, 37, 38} In
155 both systems the flows of hydroxyl radical precursor, acetaldehyde and bath gas (He, He/ O_2 , N_2 , N_2/O_2)
156 were regulated via calibrated mass flow controllers, mixed and flowed into a stainless steel 6-way cross
157 reactor. For ambient and low temperature studies, the reactor had been welded into a metal bath such that
158 just the end flanges of the cell arms protrude through the walls of the bath. Low temperature measurements
159 at 212 K were obtained by filling the bath with chloroform/dry ice. For studies at 385 K, a different reactor
160 was heated with a ceramic oven which was custom made to fit around the central portion of the reaction
161 cell. The total pressure in the cells (1– 60 Torr) was regulated via a needle valve on the output line to the
162 pump and measured using a capacitance manometer. The temperature close to the reaction zone was
163 measured using K-type thermocouples.

164 OH radicals were generated from the excimer laser pulsed photolysis of t-butyl hydroperoxide at
165 248 nm.³⁹



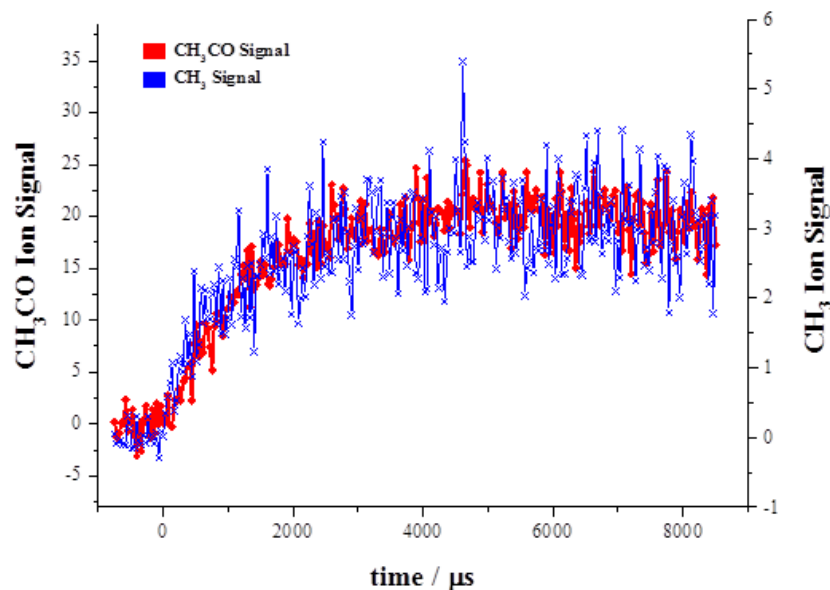
167 Photolysis energies were typically 30 - 100 mJ pulse⁻¹, the laser beam had an area of $\sim 1 \text{ cm}^2$ and was
168 introduced through one of the arms of the reactor. The laser was typically operated at 10 Hz, although
169 some studies were carried out at lower repetition rates to check that fresh gas was present for each
170 photolysis pulse.

171 OH radicals were detected by off-resonance LIF (details in the ESI). The time delay between the
172 photolysis and probe lasers was controlled by home-written software and was varied to build up a record
173 of the OH signal following photolysis. Kinetic traces (e.g. inset to Fig 5) were typically 200 – 400 data
174 points each averaged 2 - 10 times depending on the signal-to-noise ratio.

175

177 Initial PIMS Results Demonstrating CH₃ Production

178 Many previous product studies on reaction 1 have operated under conditions where there is no time
 179 resolution on the reaction products. In these circumstances it is not possible to temporally correlate reagent
 180 removal with product production. However, in our PIMS studies the primary reaction has been isolated
 181 and Figure 1 shows an example of the acetyl and methyl signals recorded in the same experiment. Clearly
 182 there can be no doubt that they originate from the same source.



183

184 **Figure 1.** Overlaid plots of acetyl (♦) and methyl (×) signal from the same experiment (1.5 Torr He, N₂O/H₂O as
 185 the OH source, [CH₃CHO] = 4 × 10¹³ molecule cm⁻³) showing that they are produced on the same timescale.

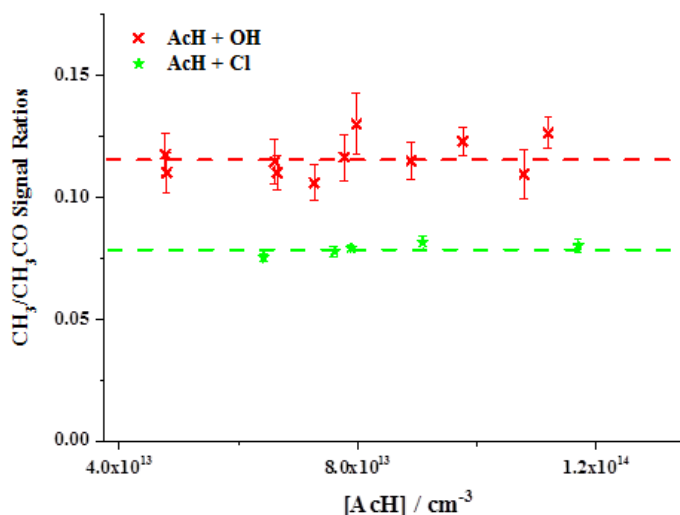
186

187 However, Figure 1 in itself does not confirm methyl as the direct product of reaction 1 as methyl
 188 ions are formed during the acetyl photoionization process. Figures 2 and 3 qualitatively show that acetyl
 189 fragmentation is not the sole source of methyl ion signal. In Figure 2 the ratio of signal height (the *S*
 190 parameter from E1) at *m/z* 15 (CH₃): *m/z* 43 (acetyl) is shown with acetyl radicals being generated from
 191 the reactions of OH or Cl with acetaldehyde:



193 The higher ratio from reaction 1 is explained by the fact that acetyl radicals produced from reaction 9 do
 194 not possess sufficient energy (requires 71 kJ mol⁻¹) to fragment further to CH₃ and CO. The 15:43 ratio
 195 from reaction 9 is therefore solely due to fragmentation in the photoionization process. However, in

196 reaction 1 the 15:43 ratio is higher as the m/z 15 signal is produced both by fragmentation and by methyl
197 radical production from reaction 1.



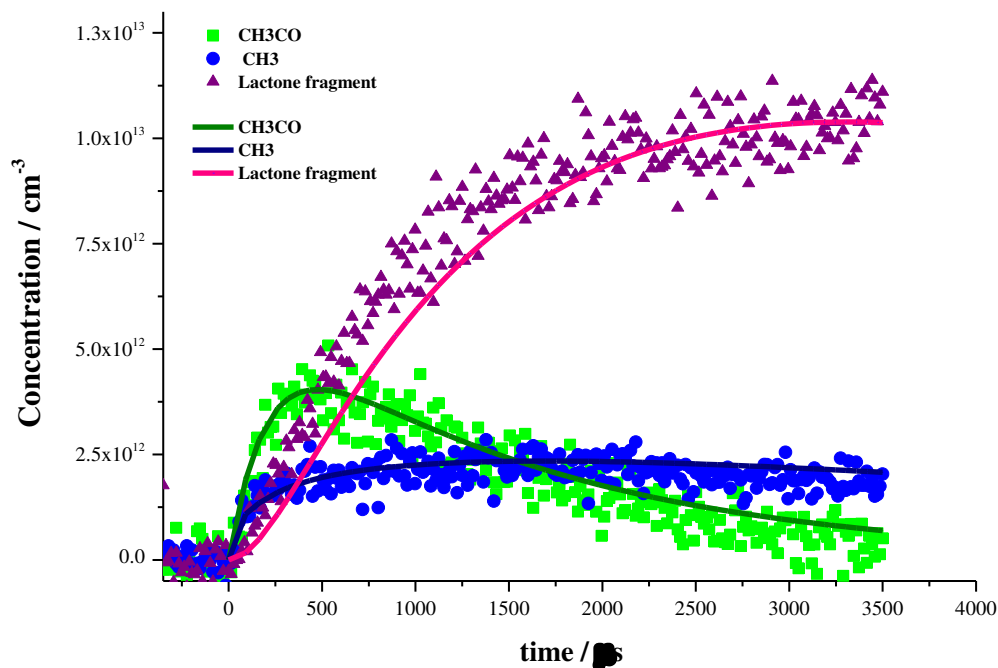
198

199 **Figure 2.** Methyl:acetyl signal ratios following the reaction of OH with acetaldehyde (AcH) and Cl with
200 acetaldehyde. The dashed lines are the average values in these experiments.

201

202 In Figure 3, a small amount of oxygen (~ 10 mTorr) was present in the system and hence a
203 significant fraction of the acetyl that survived fragmentation in reaction 1e formed energized acetylperoxy
204 radicals (reaction 2b) which under the low pressures of the PIMS flowtube (~ 1.5 Torr) yielded OH and a
205 lactone (observable in our system as $m/z = 42$) with virtually 100% yield.³² The OH went on to react with
206 acetaldehyde forming a chain system where radicals are maintained for several ms. Each time the chain
207 was propagated a fraction of reaction 1 generated methyl, which accumulated (as $\text{CH}_3 + \text{O}_2$ was slow
208 under these conditions) whilst the primary acetyl product was recycled. Figure 3 shows the methyl and
209 acetyl radical concentrations which clearly behave very differently as a function of time. The solid lines
210 in Figure 3 are simulations from a numerical model of the system, details of which are given in Section
211 3.0 of the ESI. Whilst we have fitted the magnitudes of the signals to the observed data (as sensitivity
212 factors are not available for lactones etc), no attempt has been made to fit the temporal behavior of the
213 signals. Given the uncertainties in some of the rate coefficients and in the concentration of O_2 , we believe
214 the agreement to be satisfactory. The main result from Figure 3 is that the CH_3 and CH_3CO signals show
215 different temporal profiles demonstrating that fragmentation is not the sole source of the $m/z=15$ signal.

216



217

218 **Figure 3.** Behavior of acetyl, methyl and lactone signals in an OH/CH₃CHO/O₂ system. The solid points are the
 219 experimental data and the lines are a numerical simulation based on a kinetic model. Details of the model can be
 220 found in the ESI.

221

222 Quantitative Methyl Radical Yields from Reaction 1 using the PIMS system

223 i) *Kinetics* – The PIMS apparatus can be used to obtain quantitative data on the kinetics of OH and Cl
 224 reactions with acetaldehyde. OH radicals were generated indirectly following the reaction of O(¹D) with
 225 water:



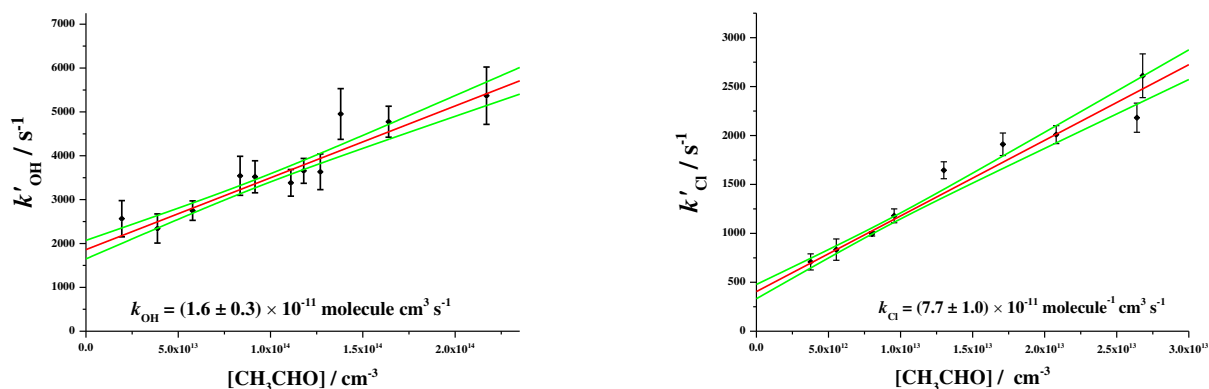
227 with O(¹D) being generated from either the 248 nm photolysis of ozone or the 193 nm photolysis of N₂O:



230 Water is the ideal hydrogen source for OH generation as, in comparison to other potential sources, e.g.
 231 H₂, the co-product of reaction 10 is also OH and water is an excellent vibrational quencher of OH.

232 Figure 4a shows an example of a bimolecular plot for the OH + acetaldehyde reaction where OH
 233 has been generated from the 248 nm photolysis of an ozone/water precursor and the reaction was followed
 234 by monitoring acetyl radical production. Examples of other data are presented in Table 1 and compared
 235 with literature data. Figure 4b shows an example of a bimolecular plot for Cl + acetaldehyde. Relatively

236 low concentrations of acetaldehyde have been used so that the resulting pseudo-first-order rate
237 coefficients are generally less than 8000 s^{-1} meaning that minimal corrections need to be made to the data
238 to account for transport effects.³⁴ Agreement with the literature is within the combined experimental
239 uncertainty in all cases. The kinetic data are in good agreement with the literature and encompass a range
240 of different measurement regimes including different precursors, detectors, laser powers, and
241 coated/uncoated reactor walls. The precision of the measurements is somewhat lower than that from
242 experiments in which the removal of OH or Cl is measured, but this is typical of a majority of studies
243 where products are monitored. The good agreement with the literature demonstrates that the target
244 reactions have been isolated and are well characterized.



245 **Figure 4.** Bimolecular plots of (a) OH + CH₃CHO, (b) Cl + CH₃CHO monitoring acetyl production.

246

247

248 **Table 1.** Measured Rate Coefficients for Reactions 1 and 9

| OH + CH ₃ CHO | | Cl + CH ₃ CHO | |
|---|--|--------------------------|--|
| Set up | 10 ¹¹ k ₁ ^a | Set up | 10 ¹¹ k ₉ ^a |
| O ₃ ^b , OD ^c , | 2.0 ± 0.2 | 248 nm ^f , OD | 6.3 ± 0.7 |
| O ₃ , OD | 1.6 ± 0.3 | 193 nm, OD | 8.6 ± 1.0 |
| O ₃ , OD | 1.5 ± 0.7 | 193 nm, ND | 8.2 ± 2.2 |
| O ₃ , OD | 1.6 ± 0.3 | 193 nm ND | 7.7 ± 1.0 |
| N ₂ O ^d , OD | 1.2 ± 0.2 | | |
| N ₂ O, ND ^e | 1.4 ± 0.3 | | |
| Average | 1.6 ± 0.2 | Average | 7.7 ± 0.7 |
| Literature ¹³ | 1.5 ± 0.2 | Literature | 8.0 ± 1.4 |

249 ^a units cm³ molecule⁻¹ s⁻¹. ^b O(¹D) from O₃ photolysis at 248 nm. ^c Old Detector. ^d O(¹D) from N₂O
 250 photolysis at 193 nm. ^e New Detector. ^f Cl generated from oxalyl chloride photolysis at either 248 or 193
 251 nm.

252

253 ii) *Methyl Fragmentation Ratios @ 248 nm* – Figure 2 clearly shows a raised CH₃:CH₃CO ratio when OH
 254 reacts with acetaldehyde in comparison to Cl reactions, however the ratio of signals cannot be simply
 255 used to calculate the direct production of methyl radicals from reaction 1e as the ionization efficiencies
 256 of CH₃⁺ from fragmentation of acetyl and from methyl itself will not be the same. Calibration was
 257 performed by using acetyl chloride as the Cl photolysis source (248 nm) in the presence of acetaldehyde
 258 and comparing the prompt acetyl and methyl signals with those produced at longer times from the Cl +
 259 acetaldehyde reaction. In the photolysis step the CH₃ signal comes from both direct methyl production
 260 and CH₃CO fragmentation. At longer times the CH₃ is solely from the fragmentation of CH₃CO formed
 261 from reaction 9. Details of the calibration procedure can be found in the ESI.



264 Using this method a methyl radical yield of (15.5 ± 6.1) % was determined for reaction 1.

265

266 iii) *Methyl Fragmentation Ratios @ 193 nm* – For the experiments performed using 193 nm photolysis a
 267 different methodology was used to calculate the yield of CH₃ from acetyl decomposition. Here, the

268 photolytic behavior of acetone at 193 nm, which is well understood⁴⁰, was used to determine the yield of
269 methyl radicals.



271 As with the experiments performed at 248 nm, the ethanal + OH and ethanal + Cl reactions were
272 investigated. However, at 193 nm these experiments were carried out back-to-back with some acetone
273 photolysis experiments. Further information is available in the ESI.

274 For these experiments a yield of methyl radicals of (14.2 ± 2.4) % was determined. The calculated
275 yield is not significantly different from the methyl radical yield determined at 248 nm, so the two
276 methodologies used appear to compare well to each other. A full list of all the experiments performed is
277 presented using in Table 2.

278 In the photolysis experiments a potential complication could arise if not all the $\text{O}(^1\text{D})$ reacted with
279 water or if any vibrationally excited OH were to react with acetaldehyde. Details of experiments to
280 investigate the magnitude of any such corrections can be found in the ESI and the slightly amended values
281 for the CH_3 yields are presented in the last column of Table 2 (Note: correction factor may be a
282 overestimation of the $\text{O}(^1\text{D})$ contribution).

283
284 **Table 2.** Methyl Radical Yields from the OH + CH₃CHO reaction.

| Method | CH ₃ Yield (%) | Corrected CH ₃ Yield (%) |
|--------------------------------------|---------------------------|-------------------------------------|
| Preliminary data (N ₂ O)* | 19.9 ± 6.0 | 17.3 ± 3.0 |
| O ₃ , OD | 15.5 ± 6.1 | 14.2 ± 5.8 |
| N ₂ O, OD | 17.1 ± 2.9 | 14.5 ± 2.0 |
| N ₂ O, ND | 14.2 ± 2.4 | 11.9 ± 1.8 |
| Average (±2σ) | 15.6 ± 2.9 | 13.5 ± 2.8 |

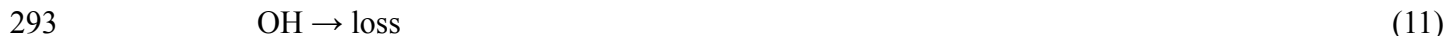
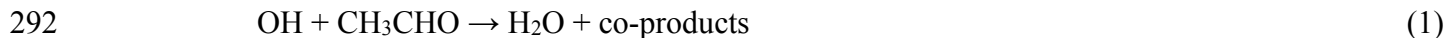
285 *data excluded from average.

286

287 **OH yields from kinetic analysis of the OH+CH₃CHO reaction with and without additional oxygen**

288 The kinetic studies of reaction 1 (with or without additional oxygen) were carried out under pseudo-first-
289 order conditions such that the concentration of acetaldehyde (and oxygen if used) was always in great

290 excess over the OH. Under these conditions, with nitrogen (or helium) as the bath gas, OH removal is
291 determined by the following reactions:

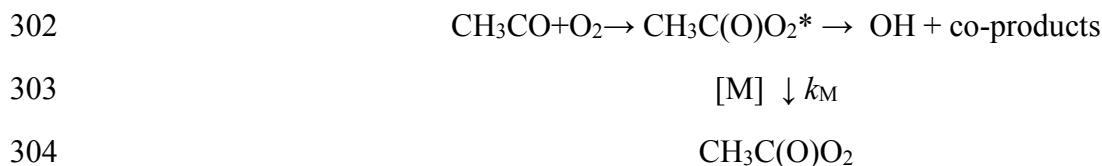


294 where reaction 11 accounts for the reaction of OH with the precursor or diffusion out of the observation
295 region. The time dependence of the OH signal I_f is given by:

296
$$I_f(t) = I_f(0)e^{-k't} \quad (E2)$$

297 where $I_f(0)$ is the initial OH signal and $k' = k_1[\text{acetaldehyde}] + k_{11}$ and therefore k_1 is the gradient of a
298 bimolecular plot (k' vs [acetaldehyde]), an example of which can be seen as the upper line in Figure 5.

299 In the presence of molecular oxygen, acetyl formed in reaction 1a will react with O_2 , with a fraction
300 regenerating OH (e.g. reaction 2b) as described above. A schematic of the acetyl + O_2 system is shown
301 below:



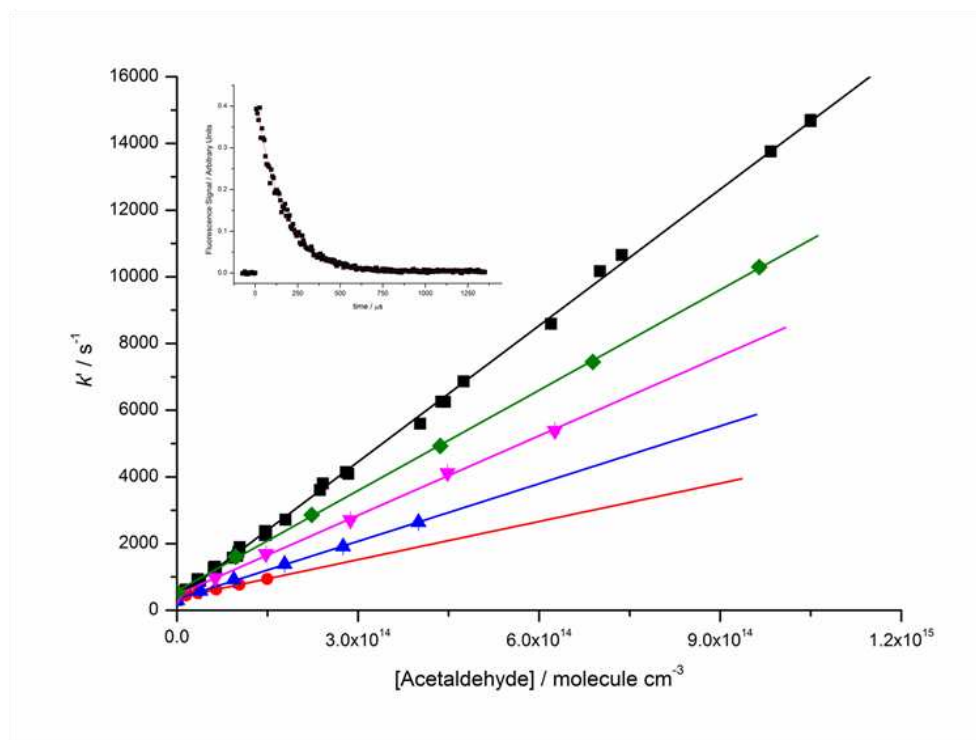
305 If the concentration of O_2 is such that the acetyl + O_2 reaction is fast compared to the OH +
306 acetaldehyde reaction ($k'_2 > 10k_1$), then under these conditions, the OH chemical removal will be
307 determined by fraction of reaction 1 that does not regenerate OH. The bimolecular rate coefficient for OH
308 loss in the presence of oxygen, k_{O_2} , will be reduced compared to nitrogen, k_{N_2} , (see lower traces in Figure
309 5). The yield of OH, Φ_{OH} , is given by:

310
$$\Phi_{\text{OH}} = 1 - \frac{k_{\text{O}_2}}{k_{\text{N}_2}} \quad (E3)$$

311 OH yields from reaction 1 were determined as a function of pressure at 212, 298 and 385 K. Φ_{OH} decreases
312 with increasing pressure due increased collisional deactivation of the initially excited $\text{CH}_3\text{C}(\text{O})\text{O}_2^*$ adduct
313 and Φ_{OH} can be parameterized with a Stern Volmer analysis (Φ_{OH}^{-1} vs [M]) where the gradient is ratio of
314 rate coefficients for $\text{CH}_3\text{C}(\text{O})\text{O}_2^*$ forming OH and being stabilized (k_M/k_T) and the intercept is Φ_{OH}^{-1} at
315 zero pressure. For the $\text{CH}_3\text{CO} + \text{O}_2$ system all studies^{e.g. 41, 42} have shown unit intercept, i.e. $\Phi_{\text{OH}} = 1$ at
316 zero pressure.

317 Figure 6 shows the Stern Volmer plots for the three temperatures studied and the results are
318 tabulated in Table 3. In all cases the confidence intervals for the intercept do not include, and are greater

319 than unity (1.04 – 1.36). An intercept > 1 suggests that a fraction of the reaction 1 is generating a product
 320 which does not regenerate OH in the presence of O₂ at low total pressures. For 298 K, the fraction of
 321 reaction (1) not regenerating OH is (18 ± 5) %.



322

323 **Figure 5.** Bimolecular plots at 298 K. (■) = no oxygen, (◆) 10 Torr O₂, (▼) 5 Torr O₂, (▲) 2 Torr O₂, (●) 1 Torr
 324 O₂; error bars are purely statistical at the 2σ level.

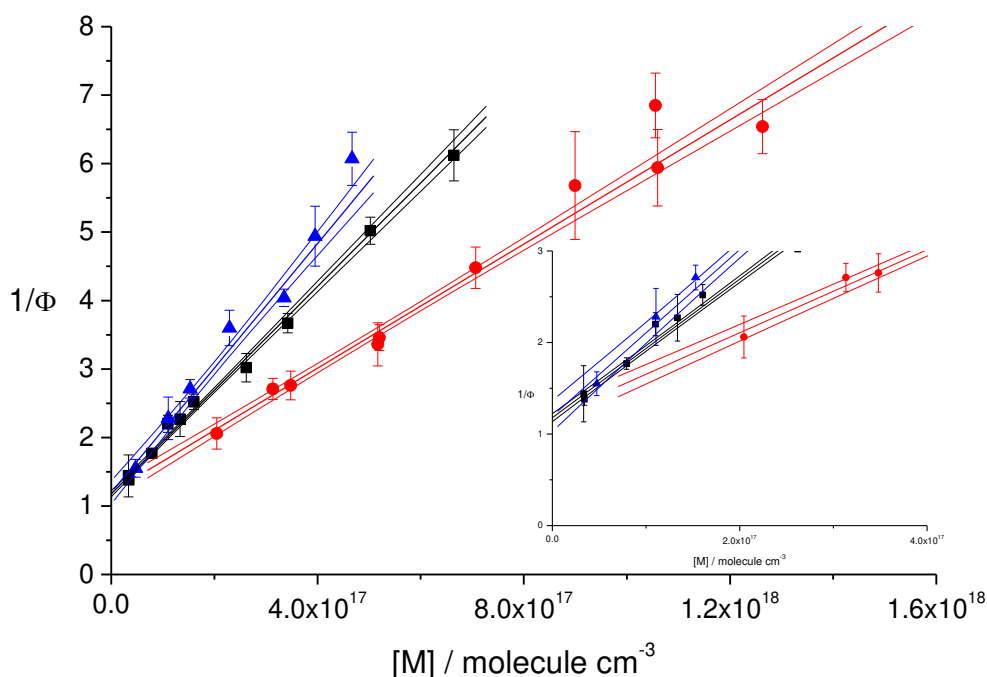
325

326 **Table 3.** Rate coefficients and Stern Volmer parameters determined for reaction 1.

| Temperature /K | $10^{11} k_1^a$ | Intercept | Max and Min Intercept | 10^{18} gradient ^c |
|----------------|-------------------|-----------|-----------------------|---------------------------------|
| 212 | 2.07 ± 0.31^b | 1.20 | 1.33 1.06 | 9.1 ± 1.3^b |
| 298 | 1.35 ± 0.13 | 1.18 | 1.23 1.13 | 7.57 ± 0.32 |
| 385 | 1.27 ± 0.24 | 1.20 | 1.36 1.04 | 4.53 ± 0.26 |

327 ^a units cm³ molecule⁻¹ s⁻¹. ^b 2σ statistical error. ^c units cm³ molecule⁻¹

328



330

331 **Figure 6.** Stern Volmer plots of the reciprocal of the OH yield vs total pressure of nitrogen. (\blacktriangle) = 212 K, (\blacksquare) = 298
 332 K, (\bullet) = 385 K. Outlying lines are 95% confidence limits.

333

334 As shown in Table 3, the bimolecular rate coefficients measured for reaction 1 are in good agreement with
 335 the recommended literature values¹³ and the measured gradient of the Stern-Volmer plot at 298 K is in
 336 reasonable agreement with earlier work from Tyndall et al.⁴³ As would be expected the gradient of the
 337 Stern-Volmer plot, the ratio of the rate coefficient for OH formation from chemically activated
 338 $\text{CH}_3\text{C}(\text{O})\text{O}_2$ to that of stabilization, decreases with increasing temperature.

339

340 Master Equation Calculations

341 In order to support the experimental observations, master equation calculations were performed using the
 342 open source code MESMER (<http://sourceforge.net/projects/mesmer/>). This software, and the basic
 343 techniques it uses to solve the chemical master equation, have been well documented elsewhere³⁶ and will
 344 not be discussed further in the current work.

345 One aspect of the MESMER functionality which is used in the current work, and does warrant
 346 additional discussion, is the use of a prior distribution statistical model in order to calculate the activated
 347 energy distribution in the CH_3CO radical following hydrogen abstraction from CH_3CHO by OH. A prior

348 distribution is one extreme example of how reaction exothermicity can be distributed and is usually
349 applied to reactions proceeding via the formation of a long-lived complex. As described below, the prior
350 distribution of energy had to be modified to selectively channel energy into the H₂O fragment (i.e. closer
351 to the dynamical picture where energy is partitioned into the newly formed bond).

352 The probability the CH₃CO product is formed with energy E ($P(E)$) is given by the following
353 expression⁴⁴:

$$354 \quad P(E) = \frac{\rho(E)[\rho_t \otimes \rho_{\text{H}_2\text{O}}](E_x - E)}{[\rho_{\text{CH}_3\text{CO}} \otimes \rho_t \otimes \rho_{\text{H}_2\text{O}}]E_x} \quad (\text{E4})$$

355 where E_x is the exothermicity of the CH₃CHO + OH reaction, $\rho_{\text{H}_3\text{CO}}$ is the ro-vibrational density of states
356 of CH₃CO, ρ_t is the classical translational density of states of the CH₃CO and H₂O fragments, $\rho_{\text{H}_2\text{O}}$ is the
357 ro-vibrational density of states of the H₂O co-product and \otimes represents a convolution. In this work the
358 classical translational density of states is used with $\rho_t \propto E$.

359 In order to refine both the exothermicity of the CH₃CHO + OH reaction and the activation energy
360 for the C-C bond dissociation in CH₃CO, electronic structure theory calculations were performed. These
361 consisted of geometry optimizations at the M062x/6-311+(3df,2pd) level of theory⁴⁵ using the Gaussian
362 09 suite of software⁴⁶ followed by single point energy calculations at the ROHF-UCCSD(T)-f12b/aug-
363 cc-pVQZ level of theory using Molpro.⁴⁷ From these calculations E_x was determined to be 124.9 kJ mol⁻¹
364 and the saddle point energy for the dissociation of CH₃CO was determined to be 61.7 kJ mol⁻¹ including
365 a zero point energy correction. In addition, in both CH₃CO and the corresponding dissociation transition
366 state (TS1), one of the vibrational normal modes corresponds to an internal hindered rotation, and
367 hindrance potentials for each of these were calculated using relaxed scans at the M062x/6-31+G** level
368 of theory. Values for $\langle \Delta E_{\text{down}} \rangle$ of 150 cm⁻¹ and 300 cm⁻¹ were used for He and N₂ respectively.⁴⁸

369 To account for the loss of the CH₃CO radical due to reaction with O₂ in MESMER, the reaction
370 was treated as a pseudo-isomerization using the methodology recently developed by Green and
371 Robertson.⁴⁹ This approach allows bimolecular reactions to be included in the master equation in a fully
372 reversible manner such that detailed balance is satisfied. Additional master equation calculations were
373 performed in order to explore the way in which the internal energy of the CH₃CO radical affected the
374 product yields upon addition of O₂. For these calculations, the potential energy surface from a previous
375 publication on the CH₃CO + O₂ reaction was used.³² The master equation calculations were performed
376 exactly as described previously with the exception that the CH₃CO fragment was initialized with a prior
377 distribution of energy as described above.

379 **DISCUSSION**

380 Our results from the PIMS measurements of methyl yields and the more indirect kinetic studies generate
381 consistent results. In combination with master equation calculations, zero pressure yields of 12 – 20%
382 have been measured for the fraction of reaction 1 leading to $\text{CH}_3 + \text{CO} + \text{H}_2\text{O}$. These results are in
383 agreement with a majority of previous product studies which conclude that abstraction is the dominant
384 mechanism, but conflict with a model of a classical abstraction process and with the methyl yield
385 determinations of Wang et al.²² and Cameron et al.²¹ These are not easy experiments and therefore we
386 have tried to ensure that our PIMS results are not subject to systematic errors by using different OH
387 precursors and repeating the experiments under a range of different conditions (e.g. coated or uncoated
388 walls, different detectors, wide range of acetaldehyde concentrations, varying radical densities), and by
389 ensuring that we can reproduce literature values for OH and Cl rate coefficients with acetaldehyde.

390 The qualitative data on the PIMS methyl yields clearly show that methyl radicals are not solely
391 generated from acetyl fragmentation and therefore the correlation in the kinetics between methyl and
392 acetyl production demonstrates that methyl is being generated directly from reaction 1. There are other
393 possible sources of methyl radicals (detailed in the ESI); for example if insufficient water is added, then
394 acetaldehyde can compete with water for the $\text{O}(^1\text{D})$ produced from ozone or nitrous oxide photolysis:



396 However, the fast timescale of $\text{O}(^1\text{D})$ chemistry means that methyl radicals produced in this way will
397 appear as an instant growth rather than on the same time scale as acetyl radicals. Conversely, because of
398 the low overall radical concentrations, any radical-radical reactions leading to methyl production would
399 occur on much longer timescales than acetyl generation. However, the yield of methyl radical determined
400 would be dependent on acetaldehyde concentration and this was not observed experimentally.
401 Additionally, the potential for interference from vibrationally ‘hot’ OH was also investigated (see
402 supplementary information for details), with the modeling of this effect suggesting an [acetaldehyde]
403 dependency which was not observed experimentally. The results from the modeling of these reaction
404 channels implies that the dominant source of methyl radicals is the chemically activated decomposition
405 of acetyl radicals.

406 The kinetic studies are more indirect in nature, but are complementary to the more direct
407 observation of methyl yields and thus help to eliminate possible systematic errors. For example reaction
408 5, ($\text{CH}_3\text{CO} + \text{O}_3$) could be a source of methyl in some of the PIMS experiments, but no ozone is present

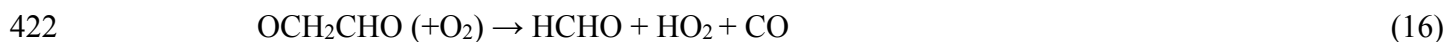
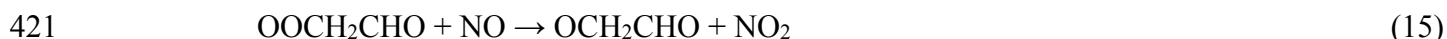
409 in the kinetic studies. The increase in the intercept of the Stern Volmer plot above unity merely gives a
410 measure of the fraction of the reaction 1 that does not recycle OH radicals, predominantly via reaction 2,
411 ($\text{CH}_3\text{CO} + \text{O}_2 \rightarrow \text{OH} + \text{co-products}$). Channel 1e ($\text{CH}_3 + \text{CO} + \text{H}_2\text{O}$) is one possibility, but another is the
412 abstraction from the methyl group of acetaldehyde, reaction 1d, generating the vinoxy radical:



414 with a yield of $\sim 5\%$ determined by Butkovskaya et al.²⁰, a value which cannot account for our observations
415 (which suggests an $(13.5 \pm 2.8)\%$ non-OH recycling component from the PIMS studies) and additionally
416 the reaction of vinoxy with O_2 may actually regenerate OH via reaction 13.^{50, 51}



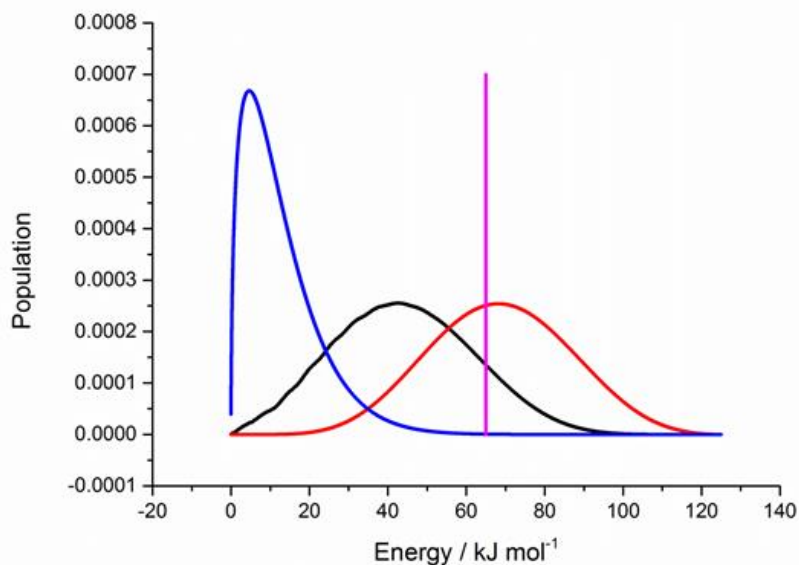
418 Reactions 13 and 14-16 would also provide a partial explanation for the results of D'Anna et al.²⁶
419 who observed a 10% yield of HCHO and CO in a chamber study at 760 Torr.



423 However, once again, the observed yield of HCHO and CO is greater than the initial vinoxy yield from
424 reaction (1d).

425 Not surprisingly, when performing master equation calculations on the dissociation of the
426 activated CH_3CO radical, it was found that partitioning the exothermicity from the $\text{CH}_3\text{CHO} + \text{OH}$
427 reaction (-123 kJ mol^{-1}) on a purely statistical basis over predicted the yield of CH_3 and CO, giving a
428 branching ratio of 83%. In order to model the experimental data, it was found that the amount of energy
429 deposited in the CH_3CO needed to be reduced. The prior distribution was altered though increasing the
430 density of states of the H_2O and vibrational modes were added to this species until MESMER simulations
431 in 1.5 Torr of He predicted a dissociation yield of $\sim 14\%$, in agreement with experiment. Vibrational
432 energy distributions from the modified prior distribution are shown in Figure 7. Note the good agreement
433 between the peak of the calculated water distribution and the average internal energy of water measured
434 by Butkovskaya and Setser.⁵²

435



436

437 **Figure 7.** Energy distributions in acetyl (black line), H₂O (red line) and in translational motion of the fragments
 438 (blue line) calculated using a prior distribution calculation modified to give 13.6% acetyl fragmentation at 1.5 Torr
 439 He and 298 K. The pink line indicates 52% of the total reaction exothermicity (124.9 kJ mol⁻¹) which is the
 440 proportion of the energy measured to go into the H₂O by Butkovskaya and Setser.⁵²

441

442 The calculated dissociation yields were found to be dependent upon both pressure and the value
 443 used for the energy transfer parameter $\langle \Delta E_{\text{down}} \rangle$. Further details are available in the ESI. It was found that
 444 the CH₃ yield decreases with both increasing pressure and $\langle \Delta E_{\text{down}} \rangle$ and this can readily be rationalized in
 445 terms of the increased rate of collisional stabilization of the activated CH₃CO fragments which reduces
 446 the amount of prompt fragmentation.

447 Two previous studies on reaction 1 have looked for methyl radicals. Wang et al.²² used tuneable
 448 diode laser IR absorption to monitor the production of ground vibrational state methyl radicals from
 449 reaction 1, calibrated by the known CH₃ yield from the O(¹D) reaction with methane. A prompt methyl
 450 signal was observed attributed to reaction 5 with a slower growth of methyl radicals from reaction 1 on
 451 the 100's of μsec timescale. It is not clear from the paper how the significant loss of methyl radicals from
 452 radical-radical processes, occurring on a similar timescale to methyl production or the production of
 453 vibrationally excited methyl radicals has been taken into account and therefore it is possible that the
 454 reported methyl yield at ~14 Torr of helium (5%) may be an underestimate of the yield. Using the
 455 MESMER input optimized to produce ~13.5 % CH₃ yield at 1.5 Torr of helium, it was found that
 456 increasing the pressure to 14 Torr reduced the calculated methyl yield to approximately 12 %.

457 Cameron et al.²¹ used UV absorption (200 – 240 nm) to observe acetyl and methyl radicals
458 produced in reaction 1. The acetyl absorption spectrum is quite broad and featureless in this region,
459 whereas in contrast, the ground state methyl absorption peaks sharply at ~216 nm. High concentrations
460 of acetaldehyde were used and therefore there is no time resolution in the production of acetyl or methyl
461 radicals. Methyl radicals were observed, but Cameron et al.²¹ suggest that this can be attributed to
462 acetaldehyde photolysis and the maximum yield of methyl radicals was set at 3% for the 60 Torr (N₂)
463 experiments. Uncertainties in accounting for the CH₃ photolysis yield or possible contributions from
464 vibrationally excited species could increase methyl yields and MESMER calculations suggest a reduced
465 methyl yield of 11% for 60 Torr of N₂ compared to our PIMS experiments (~1.5 Torr He).

466 Neither of the previous studies on methyl radical production are ideal to determine methyl yields
467 in the region of 5 – 15%, and indeed, were not designed to achieve such precision. At the time it had been
468 proposed that addition-elimination reactions might be the dominant pathways for the reaction of OH with
469 acetaldehyde and both studies, this work and that of D'Anna et al.²⁶, clearly demonstrate that methyl
470 radical production is a minor channel in reaction 1.

471 Despite being a minor channel, so that atmospheric implications are limited, the observation of
472 methyl radicals from reaction 1 raises some interesting points about the mechanism of abstraction
473 reactions and may have implications for low temperature combustion. Conventionally in an abstraction
474 reaction, reaction exothermicity is preferentially channeled into the newly formed bond with the acetyl
475 fragment being a 'spectator' of the reaction. The observation of ~15% fragmentation of the acetyl radical,
476 with fragmentation requiring greater than 50% of the reaction exothermicity to be channeled into acetyl,
477 demonstrates that the energy is distributed more statistically. A completely statistical distribution of energy
478 would preferentially excite the acetyl fragment (12 modes vs 3 modes) and lead to almost complete acetyl
479 fragmentation. Clearly both the classical 'dynamic' and 'statistical' models of partitioning energy do not
480 agree with our experimental observations or those of other workers. Butkovskaya and Setser⁵² have
481 studied the IR chemiluminescence arising from reaction 1 and several other abstraction reactions. Based
482 on their observations they calculate that 52% of the reaction exothermicity is channeled into vibrational
483 excitation of the water. Figure 7 shows a line corresponding to 52% of the total exothermicity and it can
484 be observed that the peak in the H₂O vibrational distribution from this work is consistent with the
485 observations of Butkovskaya and Setser. Their observations also point to significant differences in the
486 mechanism of OH abstraction reactions between alkanes and carbonyls. In the latter case a smaller fraction
487 of the reaction exothermicity (typically ~50% vs 70%) is channeled into vibration/bending of the water
488 molecule and the ratio of vibrational:bending is much more statistical following abstraction from a

489 carbonyl species. The potential for post-reaction complexes between the water and carbonyl radicals to
490 facilitate widening the distribution of energy was postulated as one possible explanation. Our observations
491 on the degree of OH recycling in the presence of oxygen following OH reaction with methylglyoxal and
492 glyoxal are also only consistent with a significant fraction of the reaction exothermicity being present in
493 the CH₃C(O)CO and HC(O)CO fragments respectively.^{27,30}

494 The implications of this study could be significant in low temperature combustion, particularly
495 under oxyfuel combustion conditions (combustion in pure oxygen to facilitate post combustion CO₂
496 capture⁵³). Aldehydes are known to be important intermediates in the combustion of alcohols and Kaiser
497 et al.⁵⁴ have modeled the chemistry of acetaldehyde oxidation under typical low temperature combustion
498 conditions ($T < 1000$ K). At temperatures below 750 K chain branching can occur via reactions 2a, 17 and
499 18:



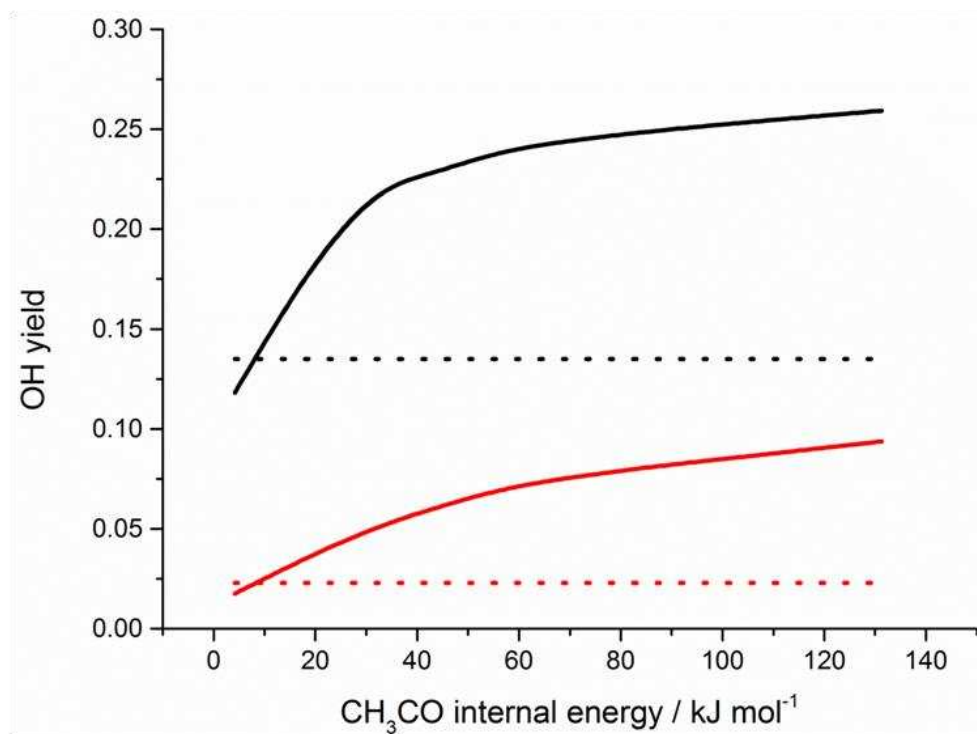
503 Reaction 2a will be in competition with the chain propagation step 2b



505 with the likely co-product being a lactone which decomposes to HCHO and CO. MESMER calculations
506 emphasize the importance of ‘well-skipping’ reactions in such R + O₂ systems⁵⁵ and well-skipping will
507 be enhanced with vibrational excitation of the R radical. Our results indicate significant vibrational
508 excitation of the acetyl fragment following reaction 1 and, particularly under oxyfuel combustion where
509 there will be less vibrational relaxation, the fraction of chain branching, reactions 2a, 17, 18, versus chain
510 propagation, reaction 2b, will change.

511 To explore how the importance of the well-skipping reactions changes with the amount of internal
512 energy in the CH₃CO fragment, calculations have been performed upon the CH₃CO + O₂ reaction with
513 the CH₃CO radical initiated with varying amounts of excess energy using a prior distribution. From these
514 calculations it is found that as the internal energy of the CH₃CO radical is increased, well-skipping
515 reactions from the excited CH₃CO increase the yield of the lactone + OH product channel relative to
516 stabilization of the RO₂ species CH₃C(O)OO. Figure 8 shows the calculated yield of OH versus the
517 internal energy in the CH₃CO, where here the internal energy of the CH₃CO is associated with the peak
518 of the distribution of energies. Such enhancements of well-skipping to yield the chain propagation

519 products compared to stabilization to give acetyl peroxy radicals and potential chain branching via
520 reactions 17 and 18, could influence modeled ignition delays for ethanal combustion.
521



522

523 **Figure 8.** Calculated OH yields from the CH₃CO + O₂ reaction at 100 (black) and 760 (red) Torr air and 298 K. In
524 these calculations the CH₃CO was initialized with a prior distribution as described above, and the excess energy
525 available was varied. The internal energy on the x axis is given by the peak in the CH₃CO initial distribution of
526 energies. The dotted lines correspond to OH yields under Boltzmann conditions at 298 K.

527

528 ASSOCIATED CONTENT

529 **Supporting Information.** Additional details on experimental techniques, the calibration methods, the
530 investigation of possible interferences from secondary chemistry and the pressure dependence of
531 calculated CH₃ yields. This material is available free of charge via the Internet at <http://pubs.acs.org>.

532

533 AUTHOR INFORMATION

534 Corresponding Authors

535 * Paul Seakins, School of Chemistry, University of Leeds, Leeds, LS2 9JT, UK, p.w.seakins@leeds.ac.uk.

536 Mark Blitz, School of Chemistry, University of Leeds, Leeds, LS2 9JT, UK, m.blitz@leeds.ac.uk.

537 Present Addresses

538 † Current address, Argonne National Laboratory, Argonne, IL, USA.⁺ Escuela de Ingenieria Industrial de
539 Toledo, Toledo, Spain. ‡ University of Bristol, Canntock's Close, Bristol, UK. # Institute of Chemistry,
540 Eotvos University, Budapest, Hungary.

541 **Author Contributions**

542 The manuscript was written through contributions of all authors.

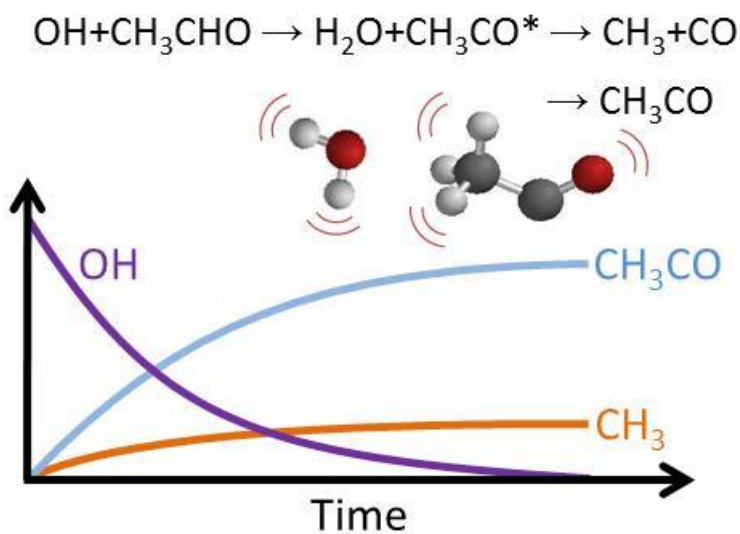
543

544 **ACKNOWLEDGMENT**

545 The authors are grateful to NERC for studentships for NUMH, and JPAL, to EPSRC for a studentship for
546 SAC (Grant GR/T28560/01) and support for RJS (Grant EP/J010871/1).

547

548 TOC



549

REFERENCES

1. D. J. Luecken, W. T. Hutzell, M. L. Strum and G. A. Pouliot, *Atmos. Environ.*, 2012, **47**, 477-490.
2. S. A. Carr, M. A. Blitz and P. W. Seakins, *J. Phys. Chem. A*, 2011, **115**, 3335-3345.
3. G. Karavalakis, T. D. Durbin, M. Shrivastava, Z. Q. Zheng, M. Villela and H. J. Jung, *Fuel*, 2012, **93**, 549-558.
4. D. B. Millet, E. Apel, D. K. Henze, J. Hill, J. D. Marshall, H. B. Singh and C. W. Tessum, *Environmental Science & Technology*, 2012, **46**, 8484-8492.
5. P. Dagaut and C. Togbe, *Fuel*, 2008, **87**, 3313-3321.
6. B. Q. He, M. B. Liu, J. Yuan and H. Zhao, *Fuel*, 2013, **108**, 668-674.
7. K. A. Read, L. J. Carpenter, S. R. Arnold, R. Beale, P. D. Nightingale, J. R. Hopkins, A. C. Lewis, J. D. Lee, L. Mendes and S. J. Pickering, *Environmental Science & Technology*, 2012, **46**, 11028-11039.
8. Y. J. Zhang, Y. J. Mu, P. Liang, Z. Xu, J. F. Liu, H. X. Zhang, X. K. Wang, J. Gao, S. L. Wang, F. H. Chai and A. Mellouki, *Atmos. Environ.*, 2012, **59**, 186-191.
9. H. K. Wang, C. H. Huang, K. S. Chen and Y. P. Peng, *Aerosol Air Qual. Res.*, 2010, **10**, 559-570.
10. S. M. Correa, G. Arbilla, E. M. Martins, S. L. Quiterio, C. D. Guimaraes and L. V. Gatti, *Atmos. Environ.*, 2010, **44**, 2302-2308.
11. E. C. Fortner, J. Zheng, R. Zhang, W. B. Knighton, R. M. Volkamer, P. Sheehy, L. Molina and M. Andre, *Atmos. Chem. Phys.*, 2009, **9**, 467-481.
12. E. P. A. US, *Health Assessment Document for Acetaldehyde.*, Environmental Criteria and Assessment Office, Office of Health and Environmental Assessment, Office of Research and Development, Research Triangle Park, NC, 1987.
13. R. Atkinson, D. L. Baulch, R. A. Cox, J. N. Crowley, R. F. Hampson, R. G. Hynes, M. E. Jenkin, M. J. Rossi and J. Troe, *Atmos. Chem. Phys.*, 2004, **4**, 1461-1738.
14. S. P. Sander, R. R. Friedl, J. P. D. Abbatt, J. Barker, D. M. Golden, C. E. Kolb, M. J. Kurylo, G. K. Moortgat, P. H. Wine, R. E. Huie and V. L. Orkin, *Chemical kinetics and photochemical data for use in atmospheric studies - Evaluation 17*, Jet Propulsion Laboratory, Pasadena CA, 2011.
15. M. Wollenhaupt, S. A. Carl, A. Horowitz and J. N. Crowley, *J. Phys. Chem. A*, 2000, **104**, 2695-2705.
16. G. Vasvari, I. Szilagyi, A. Bencsura, S. Dobe, T. Berces, E. Henon, S. Canneaux and F. Bohr, *Phys. Chem. Chem. Phys.*, 2001, **3**, 551-555.
17. P. H. Taylor, M. S. Rahman, M. Arif, B. Dellinger and P. Marshall, *Proceedings of the Combustion Institute*, 1996, **26**, 497-504.
18. S. Vandenberk and J. Peeters, *Journal of Photochemistry and Photobiology a-Chemistry*, 2003, **157**, 269-274.
19. S. Vandenberk, L. Vereecken and J. Peeters, *Phys. Chem. Chem. Phys.*, 2002, **4**, 461-466.
20. N. I. Butkovskaya, A. Kukui and G. Le Bras, *J. Phys. Chem. A*, 2004, **108**, 1160-1168.
21. M. Cameron, V. Sivakumaran, T. J. Dillon and J. N. Crowley, *Phys. Chem. Chem. Phys.*, 2002, **4**, 3628-3638.
22. J. Wang, H. L. Chen, G. P. Glass and R. F. Curl, *J. Phys. Chem. A*, 2003, **107**, 10834-10844.
23. R. J. Shannon, M. A. Blitz, A. Goddard and D. E. Heard, *Nat. Chem.*, 2013, **5**, 745-749.

24. R. J. Shannon, R. L. Caravan, M. A. Blitz and D. E. Heard, *Phys. Chem. Chem. Phys.*, 2014, **16**, 3466-3478.
25. E. Vohringer-Martinez, B. Hansmann, H. Hernandez, J. S. Francisco, J. Troe and B. Abel, *Science*, 2007, **315**, 497-501.
26. B. D'Anna, V. Bakken, J. A. Beukes, C. J. Nielsen, K. Brudnik and J. T. Jodkowski, *Phys. Chem. Chem. Phys.*, 2003, **5**, 1790-1805.
27. M. T. Baeza-Romero, D. R. Glowacki, M. A. Blitz, D. E. Heard, M. J. Pilling, A. R. Rickard and P. W. Seakins, *Phys. Chem. Chem. Phys.*, 2007, **9**, 4114-4128.
28. J. C. Polanyi, *Science*, 1987, **236**, 680-690.
29. J. Mendes, C. W. Zhou and H. J. Curran, *J. Phys. Chem. A*, 2014, **118**, 12089-12104.
30. J. Lockhart, M. Blitz, D. Heard, P. Seakins and R. Shannon, *J. Phys. Chem. A*, 2013, **117**, 11027-11037.
31. J. V. Michael, D. G. Keil and R. B. Klemm, *J. Chem. Phys.*, 1985, **83**, 1630-1636.
32. S. A. Carr, D. R. Glowacki, C. H. Liang, M. T. Baeza-Romero, M. A. Blitz, M. J. Pilling and P. W. Seakins, *J. Phys. Chem. A*, 2011, **115**, 1069-1085.
33. G. da Silva, *Phys. Chem. Chem. Phys.*, 2010, **12**, 6698-6705.
34. M. T. Baeza-Romero, M. A. Blitz, A. Goddard and P. W. Seakins, *Int. J. Chem. Kinet.*, 2012, **44**, 532-545.
35. M. A. Blitz, A. Goddard, T. Ingham and M. J. Pilling, *Rev. Sci. Instrum.*, 2007, **78**.
36. D. R. Glowacki, C. H. Liang, C. Morley, M. J. Pilling and S. H. Robertson, *J. Phys. Chem. A*, 2012, **116**, 9545-9560.
37. P. A. Cleary, M. T. B. Romero, M. A. Blitz, D. E. Heard, M. J. Pilling, P. W. Seakins and L. Wang, *Phys. Chem. Chem. Phys.*, 2006, **8**, 5633-5642.
38. D. R. Glowacki, J. Lockhart, M. A. Blitz, S. J. Klippenstein, M. J. Pilling, S. H. Robertson and P. W. Seakins, *Science (Washington, D. C., 1883-)*, 2012, **337**, 1066-1067.
39. M. Baasandorj, D. K. Papanastasiou, R. K. Talukdar, A. S. Hasson and J. B. Burkholder, *Phys. Chem. Chem. Phys.*, 2010, **12**, 12101-12111.
40. P. D. Lightfoot, S. P. Kirwan and M. J. Pilling, *J. Phys. Chem.*, 1988, **92**, 4938-4946.
41. S. A. Carr, M. T. Baeza-Romero, M. A. Blitz, M. J. Pilling, D. E. Heard and P. W. Seakins, *Chem. Phys. Lett.*, 2007, **445**, 108-112.
42. G. Kovacs, J. Zador, E. Farkas, R. Nadasdi, I. Szilagyi, S. Dobe, T. Berces, F. Marta and G. Lendvay, *Physical Chemistry Chemical Physics*, 2007, **9**, 4142-4154.
43. G. S. Tyndall, J. J. Orlando, T. J. Wallington and M. D. Hurley, *Int. J. Chem. Kinet.*, 1997, **29**, 655-663.
44. M. Baer and W. L. Hase, *Unimolecular Reaction Dynamics*, Oxford University Press, Oxford, 1986.
45. Y. Zhao and D. G. Truhlar, *Theor. Chem. Acc.*, 2008, **120**, 215-241.
46. M. J. Frisch, G. W. Trucks, H. B. Schlegel, G. E. Scuseria, M. A. Robb, J. R. Cheeseman, G. Scalmani, V. Barone, B. Mennucci, G. A. Petersson, H. Nakatsuji, M. Caricato, X. Li, H. P. Hratchian, A. F. Izmaylov, J. Bloino, G. Zheng, J. L. Sonnenberg, M. Hada, M. Ehara, K. Toyota, R. Fukuda, J. Hasegawa, M. Ishida, T. Nakajima, Y. Honda, O. Kitao, H. Nakai, T. Vreven, J. Montgomery, J. A., J. E. Peralta, F. Ogliaro, M. Bearpark, J. J. Heyd, E. Brothers, K. N. Kudin, V. N. Staroverov, R. Kobayashi, J. Normand, K. Raghavachari, A. Rendell, J. C. Burant, S. S. Iyengar, J. Tomasi, M. Cossi, N. Rega, J. M. Millam, M. Klene, J. E. Knox, J. B. Cross, V. Bakken, C. Adamo, J. Jaramillo, R. Gomperts, R. E. Stratmann, O. Yazyev, A. J. Austin, R. Cammi, C. Pomelli, J. W. Ochterski, R. L. Martin, K. Morokuma, V. G. Zakrzewski, G. A. Voth, P. Salvador,

- J. J. Dannenberg, S. Dapprich, A. D. Daniels, Ö. Farkas, J. B. Foresman, J. V. Ortiz, J. Cioslowski and D. J. Fox, *Gaussian 09, Revision A.1*, Gaussian, Inc., Wallingford CT2009.
47. H. J. Werner, P. J. Knowles, G. Knizia, F. R. Manby and M. Schutz, *Wiley Interdiscip. Rev.-Comput. Mol. Sci.*, 2012, **2**, 242-253.
 48. A. W. Jasper and J. A. Miller, *J. Phys. Chem. A*, 2011, **115**, 6438-6455.
 49. N. J. B. Green and S. H. Robertson, *Chem. Phys. Lett.*, 2014, **605**, 44-46.
 50. K. Lorenz, D. Rhasa, R. Zellner and B. Fritz, *Ber. Bunsen-Ges. Phys. Chem. Chem. Phys.*, 1985, **89**, 341-342.
 51. E. Delbos, C. Fittschen, H. Hippler, N. Krasteva, M. Olzmann and B. Viskolcz, *J. Phys. Chem. A*, 2006, **110**, 3238-3245.
 52. N. I. Butkovskaya and D. W. Setser, *J. Phys. Chem. A*, 2000, **104**, 9428-9435.
 53. M. E. Boot-Handford, J. C. Abanades, E. J. Anthony, M. J. Blunt, S. Brandani, N. Mac Dowell, J. R. Fernandez, M. C. Ferrari, R. Gross, J. P. Hallett, R. S. Haszeldine, P. Heptonstall, A. Lyngfelt, Z. Makuch, E. Mangano, R. T. J. Porter, M. Pourkashanian, G. T. Rochelle, N. Shah, J. G. Yao and P. S. Fennell, *Energy & Environmental Science*, 2014, **7**, 130-189.
 54. E. W. Kaiser, C. K. Westbrook and W. J. Pitz, *Int. J. Chem. Kinet.*, 1986, **18**, 655-688.
 55. A. J. Eskola, S. A. Carr, R. J. Shannon, B. Wang, M. A. Blitz, M. J. Pilling, P. W. Seakins and S. H. Robertson, *J. Phys. Chem. A*, 2014, **118**, 6773-6788.